基于 Pro/E的相贯曲面堆焊运动仿真分析

王新辉, 于 丹, 杨克非, 孟兆林
(机械科学研究总院 哈尔滨焊接研究所, 哈尔滨 150080)

王新辉

摘 要: 针对石油钻采专用阀门内壁复杂曲面的自动堆焊, 在堆焊设备的研发过程中, 建立了阀门内壁相贯曲线的数学模型, 规划了堆焊焊枪的运动轨迹. 在 Pro/E软件工作环境下, 建立了堆焊设备的三维实体模型, 定义了运动连接, 设定了伺服电机参数, 进行了堆焊设备虚拟样机的计算机运动仿真试验, 通过仿真分析, 生成了运动轨迹曲线并进行了仿真误差分析, 验证了该数学模型建立的正确性, 为堆焊设备的研制提供了相应的虚拟样机仿真技术支撑.

关键词: 石油钻采阀门; 相贯曲面; 运动仿真; 轨迹曲线
中图分类号: TH122 文献标识码: A 文章编号: 0253-360X(2011)02-0072-05

0 序 言

石油钻采专用阀门是石油, 天然气钻采和生产系统中的重要组成部件. 深层油气田含有大量的 H_2S, CO_2, 高氯化物等腐蚀介质, 对钻采设备, 特别是各类阀门部件具有高腐蚀性. 在阀门制造时, 内壁表层需要堆焊耐腐蚀材料[1], 既提高其耐腐蚀性, 又降低成本. 该阀门是由不同直径内圆柱表面正交或斜交产生的相贯曲面. 实现自动化堆焊具有一定难度.

在现代设计模式中, 新产品的研发采用虚拟样机技术, 通过运动仿真分析, 可以验证数学模型的准确性, 焊枪运动轨迹规划的合理性及机械系统的运动学和动力学特性, 加快研发速度和提高可靠性.

1 相贯曲线数学模型建立

通常阀体内壁相贯内圆柱面有正交, 斜交和偏交, 文中以斜交相贯为例建立相贯曲线的数学模型.

按如图 1所示建立直角坐标系, 定义垂直圆管为主管, 与主管相交的圆管分别为辅管 I 和辅管 II. 设主管所处坐标系为 $\sum O=[O; x, y, z]$, R为主管半径; 辅管 I 所处坐标系为 $\sum O_1=[O_1; x_1, y_1, z_1]$, ϕ_1为 x轴与 z轴所成夹角, d_1为 $\sum O$坐标系原点 O至 $\sum O_1$坐标系原点 O_1的距离, r_1为辅管 I 的半径; 辅管 II 所处坐标系为 $\sum O_2=[O_2; x_2, y_2, z_2]$, ϕ_2为 x轴与 z轴所成夹角, d_2为 $\sum O$坐标系原点 O至 $\sum O_2$坐标系原点 O_2的距离, r_2为辅管 II 的半径.

设主管所处坐标系 $\sum O$下的方程为

$$\sum O\{x, y, z\}: x^2+y^2=R^2 \tag{1}$$

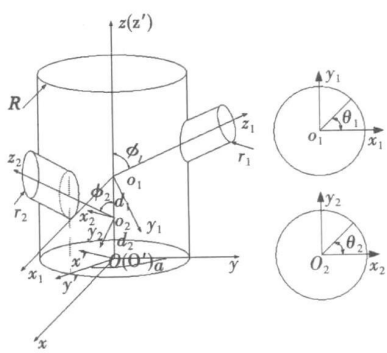

图 1 辅管主管相贯曲线图

Fig. 1 Cylinder and stack intersection curves

1.1 相贯曲线 I 数学模型

设辅管 I 所处坐标系 $\sum O_1$下的参数方程为

$$\left.\begin{aligned} x_1&=r_1\cos\theta_1\\ \sum O_1\{x_1, y_1, z_1\}: y_1&=r_1\sin\theta_1\\ z_1&=z_1 \end{aligned}\right\} \tag{2}$$

收稿日期: 2010-10-27
基金项目: 机械科学研究总院技术发展基金项目(200910126)

式中：参数 θ_1 为 $x_1O_1y_1$ 平面下的角度变量.

设 M_{o_0} 为由 $\sum O_1 \rightarrow \sum O$ 齐次坐标变换矩阵

$$M_{o_0} = \begin{bmatrix} \cos(x\text{-}x_1) & \cos(x\text{-}y_1) & \cos(x\text{-}z_1) & 0 \\ \cos(y\text{-}x_1) & \cos(y\text{-}y_1) & \cos(y\text{-}z_1) & 0 \\ \cos(z\text{-}x_1) & \cos(z\text{-}y_1) & \cos(z\text{-}z_1) & d_1 \\ 0 & 0 & 0 & 1 \end{bmatrix} \tag{3}$$

式中：$\cos(x\text{-}x_1)$ 为 x 轴与 x_1 轴夹角的余弦，其余类似；$\{0\ \ 0\ \ d_1\}^{\mathrm{T}}$ 为变换前坐标系 $\sum O_1$ 的坐标原点 O_1 在变换后的坐标系 $\sum O$ 下的坐标[2].

因此，由 $\sum O_1 \rightarrow \sum O$ 的齐次坐标变换为

$$\begin{bmatrix} x \\ y \\ z \\ 1 \end{bmatrix} = M_{o_0} \begin{bmatrix} x_1 \\ y_1 \\ z_1 \\ 1 \end{bmatrix} = \begin{bmatrix} 1 & 0 & 0 & 0 \\ 0 & \cos\phi_1 & \sin\phi_1 & 0 \\ 0 & -\sin\phi_1 & \cos\phi_1 & d_1 \\ 0 & 0 & 0 & 1 \end{bmatrix} \begin{bmatrix} x_1 \\ y_1 \\ z_1 \\ 1 \end{bmatrix} \tag{4}$$

求解矩阵方程，并联立式(2)和式(1)得

$$z_1 = \frac{\sqrt{R^2 - r_1^2\cos^2\theta_1} - r_1\cos\phi_1\sin\theta_1}{\sin\phi_1} \tag{5}$$

联立上述方程得出相贯曲线 I 参数方程为

$$\left.\begin{aligned} x &= r_1\cos\theta_1 \\ y &= \sqrt{R^2 - r_1^2\cos^2\theta_1} \\ z &= -r_1\sin\phi_1\sin\theta_1 + z_1\cos\phi_1 + d_1 \end{aligned}\right\} \tag{6}$$

式中：$0 < \phi_1 < \pi$；$0 \leqslant \theta_1 \leqslant 2\pi$；$z_1$ 为式(5).

1.2 相贯曲线Ⅱ数学模型

在图 1所示坐标系中，设辅管 II 与主管相贯所成曲线的最上端和最下端的连线与 y 轴所成平面为 $y'O'z'$，以此建立坐标系 $\sum O' = [O', x', y', z']$，且轴 y' 与 y 轴所成夹角为 α，为求此相贯曲线位于坐标系 $\sum O$ 下的参数方程，可通过 $\sum O_2 \rightarrow \sum O' \rightarrow \sum O$ 的坐标转换求得. 按照式(6)的求解方法，可解出相贯曲线 II 的参数方程为

$$\left.\begin{aligned} x &= A_1 + (A_3 - r_2\cos\phi_2\sin\theta_2)\sin\alpha\sin\phi_2 \\ y &= A_2 + (A_3 - r_2\cos\phi_2\sin\theta_2)\cos\alpha\sin\phi_2 \\ z &= -r_2\sin\theta_2\sin\phi_2 + (A_3 - r_2\cos\phi_2\sin\theta_2)\cos\phi_2 + d_2 \end{aligned}\right\} \tag{7}$$

式中：$0 < \phi_2 < \pi$，$0 \leqslant \theta_2 \leqslant 2\pi$，$0 \leqslant \alpha \leqslant 2\pi$

$$A_1 = r_2\cos\alpha\cos\theta_2 + r_2\sin\alpha\cos\phi_2\sin\theta_2$$

$$A_2 = -r_2\sin\alpha\cos\theta_2 + r_2\cos\alpha\cos\phi_2\sin\theta_2$$

$$A_3 = \sqrt{\frac{R^2 - A_1^2 - A_2^2}{\sin\phi_2} + r_2^2\cos^2\phi_2\sin^2\theta_2}$$

2 自动堆焊运动轨迹规划

为实现堆焊运动的自动化，依据式(6)和式(7)，对焊枪运动轨迹进行规划，即焊机焊接运动过程中焊枪所旋转的角度变量参数. 设区域焊道总数为 N，每条焊道宽度为 W，第 i 条焊道为 N_i；假设主管与两辅管中心线在 $\sum O = [O, x, y, z]$ 坐标系下互相垂直，即 z 轴与 z_1 及 z_2 轴所成夹角 $\phi_1 = 90^\circ$，$\phi_2 = 90^\circ$. 考虑双辅管 d_1 与 d_2 及 r_1 与 r_2 取值范围的不同，讨论以下几种情形.

2.1 两辅管在主管平面展开边界投影有相交部分

如图 2所示，将主管做平面展开后，分作五个区域进行讨论. 设运动起始点位于区域 I 的 $S(0, R, W)$ 点.

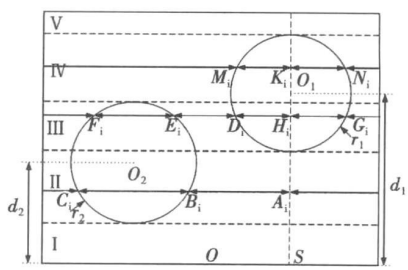

图 2 辅管投影相交时运动轨迹规划

Fig. 2 Motion trajectory planning in cross project

区域 I：$N_i W \leqslant d_2 - r_2$，焊枪距离阀体底面高度 $z_i = (N_i - 1)W$（为第 I 区域的第 i 条焊道，$i = 1, 2, 3\cdots N_1$），焊枪作全周旋转运动.

区域 II：设第 i 条焊道为 $A_iB_iC_iA_i$，有 $d_2 - r_2 \leqslant (N_1 + N_{\mathrm{II}\,i})W \leqslant d_1 - r_1$，此时焊枪距离阀体底面高度：$h_{\mathrm{II}\,i} = (N_1 + N_{\mathrm{II}\,i} - 1)W$（$i = 1, 2, 3\cdots N_{\mathrm{II}}$）. 因此根据式(7)可计算出各点 A_i，B_i，C_i 的空间坐标，根据空间两点坐标参数，可计算其距离，即

$$|A_iB_i| = \sqrt{2R^2 - 2R\left(-r_2\sin\alpha\cos\theta_{2Bi} + \cos\alpha\sqrt{R^2 - r_2^2\cos^2\theta_{2Bi}}\right)} \tag{8}$$

计算该弦长所对应的圆心角，即

$$\phi_{AiBi} = (2\times 180^\circ/\pi)\arcsin[|A_iB_i|/(2R)] \tag{9}$$

同理有 $|B_iC_i| = 2\sqrt{2}\,r_2\cos\theta_{2ci}$

$$\phi_{BiCi} = (2\times 180^\circ/\pi)\arcsin[|B_iC_i|/(2R)] \tag{10}$$

则： $\psi_{C_iA_i} = 360^\circ - \psi_{A_iB_i} - \psi_{B_iC_i}$ (11)

$\psi_{A_iB_i}$, $\psi_{B_iC_i}$, $\psi_{C_iA_i}$ 亦即焊枪在第 Ⅱ 区域运动过程中所需旋转的角度，且需满足如下关系式，即

$$\alpha = \psi_{A_iB_i} + \psi_{B_iC_i}/2$$

区域 Ⅲ：设第 条焊道为 $H_iD_iE_iF_iG_iH_i$，起始点定于 H_i 点，有 $d_1 - r_1 \leqslant (N_\mathrm{I} + N_\mathrm{II} + N_{\mathrm{III}})W \leqslant d_2 + r_2$，此时根据累积焊道总数，可计算出焊枪距离阀体底面高度：$h_{\mathrm{III}\,i} = (N_\mathrm{I} + N_\mathrm{II} + N_{\mathrm{III}\,i} - 1)W$，（$i = 1, 2, 3\cdots N_{\mathrm{III}}$）

按照区域 Ⅱ 的计算方法，可分别得出各圆心角度变量参数，即

$$|G_iD_i| = 2r\cos\theta_{1Di} \quad (12)$$

$$\psi_{GDi} = (2\times 180^\circ/\pi)\arcsin[|G_iD_i|/(2R)] \quad (13)$$

$$D_iE_i = \sqrt{2R^2 - 2P_1 r\cos\theta_{1Di} - 2P_2\sqrt{R^2 - r^2\cos^2\theta_{1Di}}}$$

式中：$P_1 = r\cos\alpha\cos\theta_{2Ei} + \sin\alpha\sqrt{R^2 - r^2\cos^2\theta_{2Ei}}$

$$P_2 = -r\sin\alpha\cos\theta_{2Ei} + \cos\alpha\sqrt{R^2 - r^2\cos^2\theta_{2Ei}}$$

$$\psi_{DiEi} = (2\times 180^\circ/\pi)\arcsin[|D_iE_i|/(2R)]$$

$$|E_iF_i| = 2\sqrt{2}r\cos\theta_{2Fi} \quad (14)$$

$$\psi_{EiFi} = (2\times 180^\circ/\pi)\arcsin[|E_iF_i|/(2R)]$$

$$\psi_{FiGi} = 360^\circ - \psi_{DiEi} - \psi_{EiFi} - \psi_{GiDi} \quad (15)$$

式中：$\theta_{1Di} = \arcsin[(d_1 - z_{Di})/r]$，且 $0 \leqslant |\theta_{1Di}| \leqslant \pi/2$；

$\theta_{2Ei} = \arcsin[(d_2 - z_{Ei})/r]$，且 $\pi/2 \leqslant |\theta_{2Ei}| \leqslant \pi$；

$\theta_{2Fi} = \arcsin[(d_2 - z_{Fi})/r]$，且 $0 \leqslant |\theta_{2Fi}| \leqslant \pi/2$；

$\theta_{1Gi} = \arcsin[(d_1 - z_{Gi})/r]$，且 $\pi/2 \leqslant |\theta_{1Gi}| \leqslant \pi$.

区域 Ⅳ：区域 Ⅳ 焊枪运动轨迹类似于区域 Ⅱ，设第 条焊道为 $K_iM_iN_iK_i$，有

$$d_2 + r_2 \leqslant (N_\mathrm{I} + N_\mathrm{II} + N_{\mathrm{III}} + N_{\mathrm{IV}})W \leqslant d_1 + r_1$$

此时焊枪距离阀体底面高度为

$$h_{\mathrm{IV}\,i} = (N_\mathrm{I} + N_\mathrm{II} + N_{\mathrm{III}} + N_{\mathrm{IV}\,i} - 1)W$$

（$i = 1, 2, 3\cdots N_{\mathrm{IV}}$）

各圆心角度变量参数为

$$|N_iM_i| = 2r\cos\theta_{1Mi} \quad (16)$$

$$\psi_{NMi} = (2\times 180^\circ/\pi)\arcsin[|2r\cos\theta_{1Mi}|/(2R)] \quad (17)$$

$$\psi_{NiKi} = \psi_{KMi} = \psi_{NMi}/2 \quad (18)$$

$$\psi_{MiNi} = 360^\circ - \psi_{NMi} \quad (19)$$

式中：$\theta_{1Mi} = \arcsin[(d_1 - z_{Mi})/r]$，且 $0 \leqslant |\theta_{1Mi}| \leqslant \pi/2$；

$\theta_{1Ni} = \arcsin[(d_1 - z_{Ni})/r]$，且 $\pi/2 \leqslant |\theta_{1Ni}| \leqslant \pi$；

区域 Ⅴ：$d_1 + r_1 \leqslant (N_\mathrm{I} + N_\mathrm{II} + N_{\mathrm{III}} + N_{\mathrm{IV}} + N_{\mathrm{V}})W$

此时焊枪距离阀体底面高度为

$$h_{\mathrm{V}\,i} = (N_\mathrm{I} + N_\mathrm{II} + N_{\mathrm{III}} + N_{\mathrm{IV}} + N_{\mathrm{V}\,i} - 1)W$$

（$i = 1, 2, 3\cdots N_{\mathrm{V}}$）

焊枪作全周旋转运动.

2.2 两辅管在主管平面展开边界投影完全重合

如图 3所示，设焊枪起始点为 S，S点坐标为 (0, R, W).

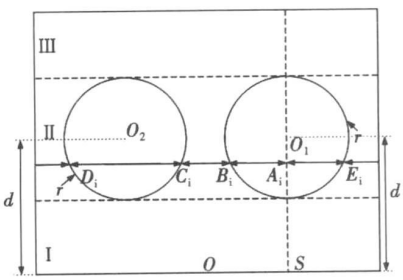

图 3 辅管投影重合时运动轨迹规划

Fig. 3 Motion trajectory planning in coincidence project

区域 Ⅰ：$N_\mathrm{I}W \leqslant d_1 - r$，焊枪距离阀体底面高度 $z_{Fi} = (N_{\mathrm{I}\,i} - 1)W$（为第 Ⅰ 区域的第 条焊道，$i = 1, 2, 3\cdots N_\mathrm{I}$），焊枪作全周旋转运动.

区域 Ⅱ：设第 条焊道为 $A_iB_iC_iD_iE_iA_i$，有 $d_1 - r \leqslant (N_\mathrm{I} + N_\mathrm{II})W \leqslant d_1 + r$，此时焊枪距离阀体底面高度：$h_{\mathrm{II}\,i} = (N_\mathrm{I} + N_{\mathrm{II}\,i} - 1)W$，（$i = 1, 2, 3\cdots N_\mathrm{II}$）

各圆心角度变量参数为

$$|E_iB_i| = 2r\cos\theta_{1Bi} \quad (20)$$

$$\psi_{EiBi} = 2\psi_{AiBi} = 2\psi_{EiAi} = (2\times 180^\circ/\pi)\arcsin[|E_iB_i|/(2R)] \quad (21)$$

$$|B_iC_i| = \sqrt{2R^2 - 2Q_1 r\cos\theta_{1Bi} - 2Q_2\sqrt{R^2 - r^2\cos^2\theta_{1Bi}}}$$

式中：$Q_1 = r\cos\alpha\cos\theta_{2Ci} + \sin\alpha\sqrt{R^2 - r^2\cos^2\theta_{2Ci}}$

$$Q_2 = -r\sin\alpha\cos\theta_{2Ci} + \cos\alpha\sqrt{R^2 - r^2\cos^2\theta_{2Ci}}$$

$$\psi_{BiCi} = (2\times 180^\circ/\pi)\arcsin[|B_iC_i|/(2R)] \quad (22)$$

$$|C_iD_i| = 2\sqrt{2}r\cos\theta_{2Di} \quad (23)$$

$$\psi_{CiDi} = (2\times 180^\circ/\pi)\arcsin[|C_iD_i|/(2R)] \quad (24)$$

$$\psi_{DiEi} = 360 - \psi_{EiBi} - \psi_{BiCi} - \psi_{CiDi} \quad (25)$$

式中：$\theta_{1Bi} = \arcsin[(d - z_{Bi})/R]$，且有 $0 \leqslant |\theta_{1Bi}| \leqslant \pi/2$；

$\theta_{2Ci} = \arcsin[(d - z_{Ci})/R]$，且有 $\pi/2 \leqslant |\theta_{2Ci}| \leqslant \pi$；

$\theta_{2Di} = \arcsin[(d - z_{Di})/R]$，且有 $0 \leqslant |\theta_{2Di}| \leqslant \pi/2$；

$\theta_{1Ei} = \arcsin[(d - z_{Ei})/R]$，且有 $\pi/2 \leqslant |\theta_{1Ei}| \leqslant \pi$.

区域 Ⅲ：$d + r \leqslant (N_\mathrm{I} + N_\mathrm{II} + N_{\mathrm{III}})W$

此时焊枪距离阀体底面高度为

$$h_{\mathrm{III}\,i} = (N_\mathrm{I} + N_\mathrm{II} + N_{\mathrm{III}} - 1)W$$

（$i = 1, 2, 3\cdots N_{\mathrm{III}}$）

焊枪作全周旋转运动.

2.3 两辅管在主管平面展开边界投影有包含部分

如图 4 所示，弧 $A_iB_iC_iA_i$、$H_iD_iE_iF_iG_iH_i$

$N_iK_iM_iN_i$上各段圆心角变量参数可分别按照两辅管投影有相交部分情况进行计算.

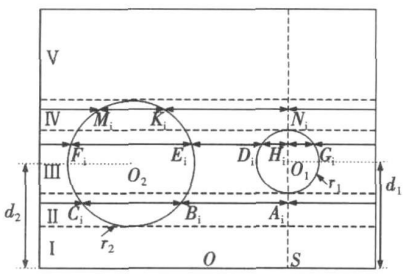

图 4　辅管投影包含时运动轨迹规划

Fig. 4　Motion trajectory planning in included project

当两辅管在主管平面展开边界投影无相交部分时可按照单管算法进行轨迹规划.

3　堆焊运动仿真分析

基于 Pro/E三维实体建模环境，建立堆焊设备各组成零部件三维实体模型，装配成虚拟整机后，如图 5所示. 对该装配体进行全局性干涉检查后，对干涉的零部件，通过修改其零件模型尺寸，调整装配约束，以消除其干涉情况，优化整机结构设计.

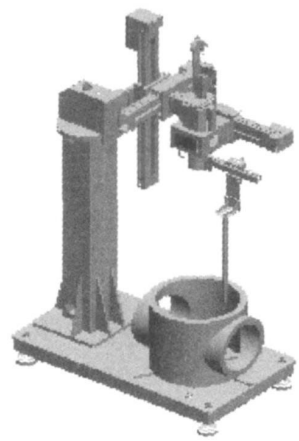

图 5　堆焊设备整机装配图

Fig. 5　Welding equipment assembly graph

如图 6所示，依据主管与辅管相贯线的位置，将阀门内壁分为 1，2，3，4四个区域，图中 A，B，C，D四点分别为 Front平面与相贯线的交点. 因此，在自动堆焊过程中，当焊枪由区域 1旋转至 A点时，焊机自动停弧，停止焊接；焊枪在区域 2中以停焊方式旋转至 B点时，焊机自动高频引弧，开始焊接；焊枪在区域 3中以焊接方式旋转至 C点时，焊机自动停弧；焊枪在区域 4中以停焊方式继续旋转至 D点时，焊机又自动引弧. 即当焊枪旋转至阀门实体时，焊机能自动高频引弧开始焊接，当焊枪旋转至相贯孔处时，焊机又能自动停弧停止焊接.

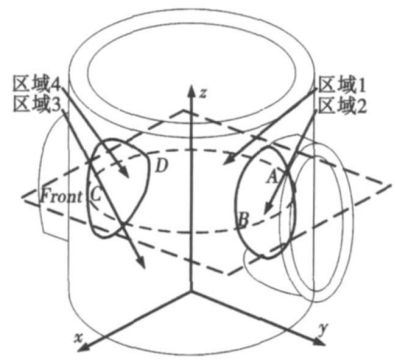

图 6　阀门示意图

Fig. 6　Sketch map of valve

为模拟焊机的堆焊运动过程，根据堆焊的工艺性及堆焊设备的设计参数要求，现设定运动仿真参数，见表 1.

表 1　运动仿真参数

Table 1　Motion simulation parameters

焊枪运动方向	焊枪提升速度 v_u/(mm·s^{-1})	焊枪旋转频率 f/(r·s^{-1})	焊枪进退速度 v_{ls}，v_D/(mm·s^{-1})	枪头初始坐标 {x，y，z}/mm	主管半径 R/mm	辅管半径 r/mm	主管高度 h/mm	焊道宽度 h_w/mm	中心距离 d/mm
正转/反转	10	0.07	10	{0，300，5}	300	200	600	10	300

将三维实体模型转入至 Pro/E机构模块进行运动仿真分析，建立运动仿真步骤如下.

（1）运动连接定义：分别定义堆焊设备竖直导轨的向上提升运动和旋转机头水平导轨的进退运动为滑动杆连接；定义旋转机头的旋转轴为销钉连接.

（2）主体定义：依据运动连接定义，系统自动分配堆焊设备主体，分别为基础主体和三个运动主体.

（3）伺服电动机定义：创建旋转轴为运动轴伺服电动机；创建竖直导轨提升几何伺服电动机；创建堆焊焊枪进给运动几何伺服电动机；创建堆焊焊枪退让运动几何伺服电动机.

（4）仿真分析定义：建立该运动仿真为位置分析以模拟机构运动，通过 MATLAB程序计算相贯线上各点坐标参数及角度变量值，设置运动帧频及快

照, 运行堆焊运动的模拟仿真.

(5)仿真结果分析: 对焊枪头运动位置变化进行测量分析, 生成焊枪枪头运动轨迹曲线, 如图 7所示.

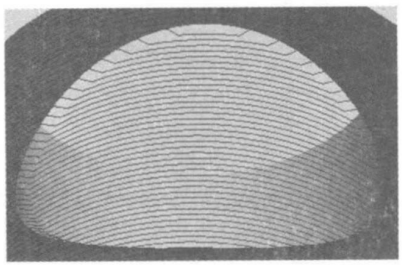

图 7 运动轨迹曲线

Fig. 7 Motion trajectory curves

由于 Pro/E机构模块中电机运行时间至多可精确识别至小数点后一位, 因此在仿真后生成的轨迹曲线在阀门相贯线处便积累了轨迹误差, 经分析其单道偏差为 0.26 mm. 在实际焊接运动过程中, 所采用的交流伺服电机驱动器为 2 500线程, 四倍频技术, 编码器脉冲当量为 360°/10 000=0.036°. 编码器有用作参考零位的 "相标志 (指示)脉冲信号, 码盘每旋转一周, 只发出一个标志信号, 该标志脉冲可用作指示机械位置或对积累量清零[3]. 因此, 实际焊接过程中的伺服电机驱动焊枪运动轨迹偏差位于误差范围之内. 仿真运动轨迹曲线满足相贯曲线数学模型及运动轨迹规划的要求.

4 结 论

(1)阀体相关线数学模型的建立及焊枪运动轨迹规划为自动化焊接运动提供了数学依据.

(2)运动仿真分析解决了阀体相贯曲面内壁难以实现自动堆焊问题, 为设备研制提供了技术支撑.

参考文献:

[1] 李 磊. 石油钻采阀门内壁热丝 TIG堆焊[J]. 石油化工建设, 2005, 12(6): 52-54.
Li Lei. Hot TIG welding of petroleum drill valve inner surface[J]. Petroleum and Chemical Construction, 2005, 12(6): 52-54.

[2] 李瑰贤. 空间几何建模及工程应用[M]. 北京: 高等教育出版社, 2007.

[3] 李科杰. 现代传感技术[M]. 北京: 电子工业出版社, 2005.

作者简介: 王新辉, 男, 1982年出生, 硕士研究生. 主要从事焊接设备的计算机模拟运动仿真及结构有限元分析. Email: xhuiwang@163.com

通讯作者: 于 丹, 男, 研究员. Email: yudan_hrh@tom.com

my Chief Equipment Ministry Laboratory of Material Interface, China University of Petroleum, Dongying 257061, China). P53—56

Abstract: By using diffusion couple made by inlaying, the diffusion layer of Al/Mg was researched under different anneal condition. The microstructure and forming rule were observed and analyzed by means of scanning electron microscopy (SEM) and Energy Disperse Spectroscopy (EDS), and its forming mechanism was discussed. The results showed that the diffusion layer was formed at Al/Mg interphase with heating temperature of 580 ℃ and holding time of 60 hours; its thickness was 265 μm; its structure was Al/Mg$_2$Al$_3$/MgAl/Mg$_3$Al$_2$/Mg which included all phases in Al/Mg binary alloy phase diagram, and the structure was consistent with the sequence of each phase located Al/Mg phase diagram. The solid phase diffusion, dissolve and crystal of Al and Mg resulted in forming of diffusion layer with different diffusion temperature and time, and the diffusion layer was almost formed at Al/Mg interphace at the same time, which was different number of layer, thickness and structure.

Key words: Al; Mg; diffusion layer; dissolve; crystal

Analysis of microstructure and binding ability of gradient coatings in controlled atmosphere DONG Xiaoqiang, LUO Chao, LI Deyuan, DUAN Sihua (School of Materials Science and Engineering, Shenyang University of Technology, Shenyang 110178, China). P57—60

Abstract: Because ceramic gradient coating with excellent performance will be affected by air oxidation effects in air atmosphere plasma spray coating preparation, Ni-Cr-B-Si/Al_2O_3 gradient coating is prepared in controlled atmosphere (argon) plasma spraying. The atmospheric conditions of making Ni-Cr-B-Si/Al_2O_3 gradient coatings are compared, and the effects of argon atmosphere on the microstructure and bonding strength of sprayed gradient coating are analyzed. The results show that the inside organization of gradient coating in argon atmospheres and in air has no obvious interface and achieves continuous change of microstructure, but the gradient coating organization in argon is more dense, lower oxidative and has higher bonding strength than that in air.

Key words: controlled atmosphere; plasma spraying; Al_2O_3 ceramic; gradient coatings; bond strength

Evaluation on interfacial fracture mode of resistance spot weld dual-phase steels YANG Haijun, ZHANG Yansong, LAI Xinmin, ZHANG Xiaoyun (1. School of Mechanical Engineering, Shanghai Jiaotong University, Shanghai 200240, China; 2. Vehicle Manufacturing Engineering, Shanghai General Motors, Shanghai 201201, China). P61—64

Abstract: The interfacial fracture mode of dual phase steel (DP) weld greatly affects its mechanical performance and decreases its weld quality because much martensite in the nugget makes the welds brittle, but the traditional nugget diameter criteria is not suitable to estimate the quality of DP weld, and so this paper builds a mathematical mode based on macro-appearance and micro-mechanism to evaluate the different fracture modes of DP weld. Experimental results show that the model is effective on 1.4 mm and 1.8 mm DP600 welds and is also better than other evaluation criteria for their limited factors considered.

Key words: dual phase steel; resistance spot welding; interfacial fracture; evaluation model

Theory and experimental research on controlling crack in double-scanning laser cladding process CHEN Lie, XIE Peilin (Department of Mechanical Engineering, Naval University of Engineering, Wuhan 430033, China). P65—68

Abstract: A new craft of laser cladding, unidirectional powder feeding and double scanning, was developped to solve the problem of cracking in the cladding coats. The temperature field and stress field of laser cladding were computed. The results indicate that the value of stress is very large and the stress concentration problem is serious at the top of cladding coat and the joint between coat and base material in the process of unidirectional scanning. After the second scanning, the value of stress can be decreased and the stress concentrated at the top of cladding coat can be eliminated. The results of laser cladding 45 steel with Ni60 alloy powder by the craft of unidirectional powder feeding and double scanning show that the cracking of the coats can be avoided both in single-pass cladding and multi-pass lap cladding by the craft which is effective and feasible for controlling crack in laser cladding.

Key words: laser technique; laser cladding; temperature field; stress field; stress concentration

Overlap model of interval bead based on GMAW forming MENG Fanjun, ZHU Sheng, BA Dema, DUWenbo (Department of Equipment Remanufacturing Engineering, The Academy of Armored Forces Engineering, Beijing 100072, China). P69—71

Abstract: The lap amount of bead is critical not only for the trouble-free operation of three-dimensional welding, but also for the forming accuracy. So the interval bead lap model of the GMAW welding is established on the basis of the physical characteristics of droplet transition. Furthermore, the theoretical bead distance of flat overlaying welding layer is calculated. Actual welding test is employed for the model verification and the height of surfacing layer also is calculated. The test results agree well with the theoretical ones, which establish the foundation for the welding automation.

Key words: three-dimensional welding; interval welding; lap amount of bead; overlaying welding layer

Analysis of intersection surface welding motion simulation based on Pro/Engineer WANG Xinhui, YU Dan, YANG Kefei, MENG Zhaolin (Harbin Welding Institute, China Academy of Machinery Science & Technology, Harbin 150080, China). P72—76

Abstract: In the development process of automatic welding equipment which is used for the complex inner surface welding in petroleum drill special-purpose valve, the mathematic model of valve inner surface intersection curve was modeled, and

the motion trajectory of welding gun was planned. The 3D model of the welding equipment based on Pro/Engineer working environment was established, the definition of the motion jointing and the parameters of servomotors were set, the virtual prototype motion simulation experiment of the welding equipment was run, the motion trajectory curve was created, and the simulation errors was analyzed. The correctness of modeling the mathematic model was validated, which provided the simulation technology supporting of virtual prototype for developing and manufacturing the welding equipment.

Key words: petroleum drill valve; intersection surface; motion simulation; trajectory curve

Extraction method of welding seam and defect in ray testing image ZHANG Xiaoguang[2], SUN Zheng, HU Xiaolei, HUAN Yuyue (1. College of Mechanical and Electrical Engineering, China University of Mining and Technology, Xuzhou 221116, China; 2. State Key Laboratory of Advanced Welding Production Technology, Harbin Institute of Technology, Harbin 150001, China; 3. Physics & Electronic Engineering Department, Zaozhuang University, Zaozhuang 277160, China). p77—80

Abstract: A practical detection method, which takes advantage of the information contained in the image itself, is presented based on local treatment gradually for attacking the difficulties in accurately detecting and extracting weld seam and defect in ray testing image. First of all, the approximate location of the weld zone in the original image is determined by detecting the regional characteristics of bands; then, the local area where the weld boundaries and defect are in is determined by analyzing gray column waveforms, and the area types are divided into the categories of non-crack and crack class roughly; finally, the detection and extraction of welding defects are realized by using the methods based on Watershed Transform and Beamlet Transform respectively. The results show that the method can accurately detect the weld boundaries and weld defect in various ray images and has good adaptability and practicality.

Key words: ray testing image; welding seam; defect extraction; Watershed Transform; Beamlet Transform

Numerical modeling of welding distortion in thin-walled mild steel pipe DENG Dean, TONG Yangang, ZHOU Zhongyu (College of Materials Science and Engineering, Chongqing University, Chongqing 400045, China). p81—84

Abstract: A thermal-mechanical nonlinear finite element method based on ABAQUS was developed to simulate the temperature, residual stress and strain fields in thin-walled structures welded by arc fusion welding processes. The welding temperature field and the welding distortion in a thin-walled mild steel pipe were predicted by using the developed finite element method. Meanwhile, experiments were carried out to measure the actual welding distortion in the thin-walled pipe welded by an arc-welding robot. The coincidence between the simulation and the experimental results confirmed the validity of the numerical simulation method. The numerical simulation method has established a foundation for prediction of welding distortion in thin-walled structure used in practical engineering.

Key words: finite element method; numerical simulation; welding temperature field; welding distortion

Microstructure and properties of rapidly solidified Ag-Cu-Sn ternary brazing fillers XU Jinfeng, ZHANG Xiaocun, DANG Bo, DAI Weigang (1. School of Material Science and Engineering, Xi'an University and Technology, Xi'an 710048, China; 2. Changshu Shuanghua Electronic Co., Ltd., Changshu 215500, China). p85—88

Abstract: The phase constitution, morphology, electrical resistivity and mechanical properties of $Ag_{42.47}Cu_{57.53-x}Sn_x$ (x= 12.23, 12.94, 13.65, mass fraction, %) prepared by melt-spun method are investigated. The results indicate that the microstructure of the alloys consists of (Ag), α-Cu and a few of $Cu_{13.7}Sn$ phases; with the rise of tin content, the electrical resistivity increases for refining of the microstructure and increasing of grain boundary amount and solute-trapping; on the other hand, fine crystal strengthening and solution hardening will result in the increment of tensile strength from 280 to 360 MPa, but the elongation reduces from 5% to 2.8%. The ranges of solidus and liquidus temperature of those alloys are 590 to 616 ℃ and 615 to 622 ℃ respectively, and the temperature range increases with the increasing of tin content.

Key words: ternary alloy; quenched brazing filler; rapid solidification; microstructure; properties

Dynamic compensation for deformation in laser welding of 3D joint seam GONG Shihua, YU Junfeng, YANG Jianzhong, LI Bin (State Engineering Research Center of Manufacturing Equipment Digitization, Huazhong University of Science and Technology, Wuhan 430074, China). p89—92

Abstract: As there is deformation perturbation in the laser welding process of 3D joint seam, the real-time measurement and dynamic compensation in the welding process is used to track accurately a 3D trajectory. The real-time measuring of the 3D joint seam welding is achieved with a laser visual sensor on a five-axis NC welding machine tool, the bias information of tracking joint seam is transformed from measuring coordinate system to workpiece coordinate system, the feed amount of axes is compensated real time, and the dynamic compensation in the welding process of 3D joint seam is realized. The stability of the loop-closed control system with 3D joint seam measuring feedback is analyzed, and the proposed arithmetic is testified by experiment, which indicates that the real-time measuring and dynamic compensation in the 3D joint seam welding process satisfies the track control requirement in 3D laser welding.

Key words: laser welding; 3D joint seam; dynamic compensation; visual sensor

Effect of $CuAl_2$ phase on properties and microstructure of Cu/Al brazed joint ZHANG Mark[2], XUE Songbai, JI Feng, LOU Yinbin, WANG Shuiqing (1. College of Materials